Study of low-profile near-field electromagnetic energy harvesting

Subash Chandra Yadav [ID] and Rajan Agrahari [ID]

Department of Electronics & Communication Engineering, NIT Patna, Patna, India

CAMBRIDGE UNIVERSITY PRESS

Abstract

In order to recover the magnetic energy that leaks from an induction cooktop, this study suggests a straightforward and cost-effective magnetic-field energy harvester (MFEH) circuit. With the aid of the intended circuitry, the acquired magnetic energy is transformed into DC electrical energy. We harvested the magnetic-field energy (MFE) from the induction cooktop at various heights and locations of the energy harvesting coil. With a load resister of 46.6 Ω and a capacitance of 1 mF, the developed MFEH circuit, when positioned 2 cm beneath the cooktop, can capture an average DC power of 1936 mW. Placing the energy-harvesting coil 7.5 cm beneath the induction cooktop lowers the power output to 142 mW. For a range of load resister values, the MFE gathered at various locations along the energy harvesting coils is examined. Batteries can be used to store the gathered energy for later use. Additionally, the suggested device is shown to be capable of wirelessly powering low-power Internet of things devices and charging mobile devices. The suggested device differs from the previously published magnetic harvesting circuits due to the induction cooktop's superior performance and capacity to gather MFE.

Introduction

The energy requirement for systems like Internet of things (IoT), wearable sensors, and biomedical devices is rising annually [1]. With limited natural resources, researchers are exploring new energy harvesting methods [2]. While ambient sources like solar and wind power large systems, they require complex, costly management and are less effective for low-power systems [3, 4]. Wireless sensor networks in IoT technology benefit from harvesting energy from cost-effective, nonnatural sources and wasted energy, offering a promising solution for powering low-power sensors [5]. The far-field RF-energy harvesting with metasurface is one of the methods to utilize the nonnatural wasted energy [6]. But they are limited with very low power (in μW range). The leaked magnetic-field energy (MFE) radiated from the induction cooktop is a nonnatural energy source and can be employed for low-power devices.

For industrial, domestic, and medical applications, induction heating (IH) is preferred over other traditional heating techniques [7–9] due to its advantage of fast heating, efficiency, and safety. In an induction cooktop, heating is produced by the induced alternating magnetic field of frequency range 20–100 kHz from the coil placed inside the cooktop. By utilizing coils and magnetic cores to trap magnetic energy, Faraday's law allows for the harvesting of these radiated magnetic fields surrounding the induction cooktop.

In the literature, low-frequency mechanical vibrations have been successfully used for magnetic-field energy harvester (MFEH) via piezoelectric and magneto-mechano-electric effects [10–13]. The overhead power lines have been utilized to capture the MFE [14]. Additionally, bus bars and power cables are other sources for the MFE [15–17] that employ various core shapes placed near power lines for MFEH. Designs such as bow ties and helical-shaped ferrite cores have been utilized to enhance output power [15, 18]. Jiang et al. [16] proposed near-field MFEH that uses power lines to store the energy for applications like low-power IoT-based sensors. Similarly, Wu et al. [17] introduced a compact and cost-effective MFEH device that couples energy via a rectangular coil. Furthermore, recently the rail currents on electrified railway tracks have been utilized for MFEH to power railway monitoring systems [19, 20]. However, MFEH from induction cooktop has not been previously explored.

The proposed low-profile MFEH circuit harvests lost energy from induction cooktops. The RF energy from the harvesting coils is converted to DC using a half-wave rectifier with a capacitor filter. DC voltage and power are measured across various load resistors and coil placements. Experimental results show that, when the coils are 2 cm below the cooktop, a DC voltage of 9.4–9.6 V and power of 1936 mW are achieved for $R_L = 46.6$ Ω. Positioned similarly, the suggested circuit yields 12.75–12.85 V and 1657 mW. Both cases use a 1 mF capacitor. Therefore, by using our proposed techniques, the leaked magnetic energies from induction cooktops can be harvested and used for low-power devices such as mobile charging and IoT-based sensors.
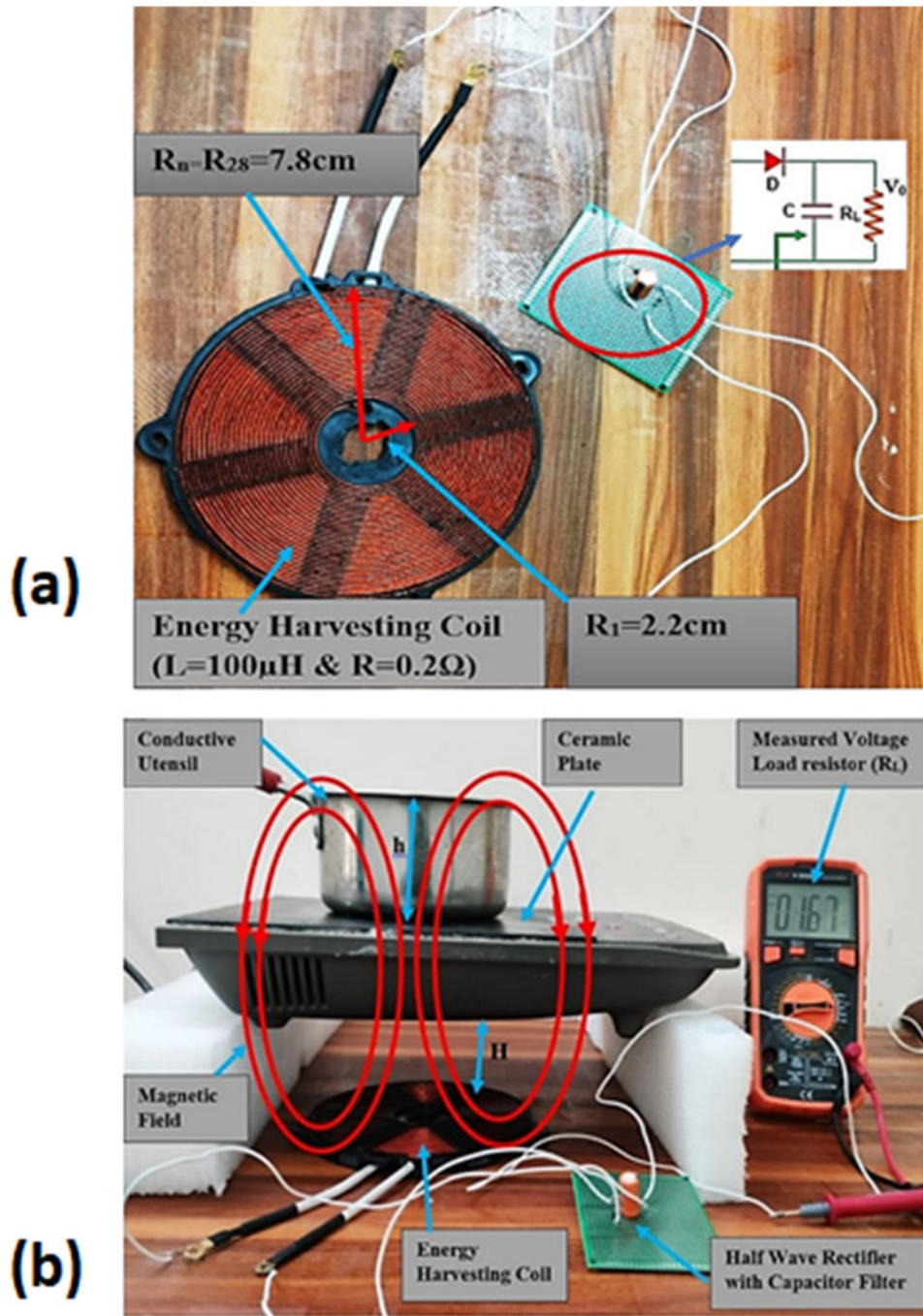
Figure 1. Structure of the energy harvesting systems of the induction cooktop and various parameters.

With the proposed circuit, energy can be stored in the battery which can be later used to power devices. In addition, the proposed circuit is capable of storing wasted nonnatural energy. The proposed circuit design is a low profile i.e., very simple and cost-effective which makes our device unique.

Theory and design

Faraday's law of electromagnetic coupling, which states that "the time rate of change of magnetic flux density of the primary coil induces the EMF in the secondary coils," is the foundation of the IH theory. Magnetic flux density (B), which is strongest at the center of the induction coils, is produced by the cooktop's induction coil. The magnetic flux generated causes a transfer of heat to the food and utensils as well as eddy current loss. Significant MFE leaks close to the induction cooktop during this procedure.

The mechanics of the suggested energy-collecting system is described in Fig. 1. The energy-collecting coil, is used to collect the induced near-field electromagnetic energy, is positioned beneath the height (H) induction coil. The induced AC voltage is converted to DC voltage at the terminal of the energy harvesting coil by a half-wave rectifier equipped with a capacitor filter. Measurements are made of the rectified DC voltage and DC power across the load. The induced voltage at the energy harvesting coil's terminal is produced by the rate at which the magnetic flux in the induction coil changes with time, as per Faraday's law of electromagnetic induction. The induced voltage (V_2) is determined by

$$V_2 = -N_2 \frac{d\psi}{dt}. \tag{1}$$

Figure 1 shows the flux ψ across a small area at a point P on an energy harvesting coil.

$$\psi = \iint \vec{B}.\vec{ds}. \tag{2}$$

Now, the vector magnetic potential $\vec{A}$ may be determined by using the curl operation to find the magnetic flux density $\vec{B}$ at point P

$$\vec{B} = \nabla \times \vec{A}. \tag{3}$$

Thus

$$\vec{A} = \oint \frac{\mu_0 I \vec{dl}}{4\pi |r_p|}. \tag{4}$$

For N_1 turns, Eq. (4) becomes

$$\vec{A} = \sum_{i=1}^{N_1} \oint \frac{\mu_0 I \vec{dl_i}}{4\pi |r_{p_i}|} \tag{5}$$

where $\vec{dl_i} = R_i d\phi \, \hat{a}_\phi$, $\vec{r_{p_i}} = r_i \hat{a}_r - R_i \, \hat{a}_\rho$ and magnitude of $|r_{p_i}| = \sqrt{r_i^2 + R_i^2 + 2r_i R_i \cos(90 + \theta_i)}$. Now, Eq. (4) is modified as

$$\vec{A} = \sum_{i=1}^{N_1} \frac{\mu_0 I 2\pi R_i}{4\pi |r_{p_i}|} \hat{a}_\phi. \tag{6}$$

Here, vector magnetic potential has only $\hat{a}_\phi$ component. Therefore,

$$A_\phi = \sum_{i=1}^{N_1} \frac{\mu_0 I 2\pi R_i}{4\pi |r_{p_i}|}. \tag{7}$$

While $A_\theta = 0$ and $A_r = 0$. The expression of magnetic flux density from Eq. (3) is given as

$$\vec{B} = \frac{1}{r_i \sin \theta_i} \left[\frac{\partial (A_{\phi_i} \sin \theta_i)}{\partial \theta_i} \right] \hat{a}_r + \frac{1}{r_i} \left[-\frac{\partial (r_i A_{\phi_i})}{\partial r_i} \right] \hat{a}_\theta. \tag{8}$$

Now, considering the B_r component in Eq. (8), we have

$$B_r = \frac{1}{r_i \sin \theta_i} \left[\frac{\partial}{\partial \theta_i} \left(\sum_{i=1}^{N_1} \frac{\mu_0 I 2\pi R_i}{4\pi \sqrt{r_i^2 + R_i^2 - 2r_i R_i \sin \theta_i}} \sin \theta_i \right) \right]$$

$$B_r = \frac{1}{r_i \sin \theta_i} \left[\left(\sum_{i=1}^{N_1} \frac{\mu_0 I 2\pi R_i}{4\pi |r_{p_i}|} \cos \theta_i \right) \right.$$

$$\left. + \left(\sum_{i=1}^{N_1} \frac{\mu_0 I 2\pi R_i^2 r_i \cos \theta_i}{4\pi |r_{p_i}|^3} \sin \theta_i \right) \right] \tag{9}$$

Figure 2. (a) Prototype of the complete circuit for MFEH and (b) measurement of DC voltage across R_L with induction cooktop and proposed circuit.

The contribution of the first term of Eq. (9) in the near field will be negligibly small. Therefore, by considering the second term of Eq. (9), we have

$$B_r = \sum_{i=1}^{N_1} \frac{\mu_0 I R_i^2 2 \cos \theta_i}{4 |r_{p_i}|^3}. \tag{10}$$

Similarly, the expression for the B_θ component is calculated as

$$B_\theta = \sum_{i=1}^{N_1} \frac{\mu_0 I R_i^2 \sin \theta_i}{4 |r_{p_i}|^3}. \tag{11}$$

If the effective cross-section area of the harvesting coil is directed along the z-direction, then the magnetic flux ψ from Eq. (2) is given as

$$\psi = \int_{R_1}^{R_{N2}} \int_0^{2\pi} (B_r \hat{a}_r + B_\theta \hat{a}_\theta) \, . r dr d\varphi \, \hat{a}_z \tag{12}$$

Here $\hat{a}_z = \cos \theta_i \, \hat{a}_r - \sin \theta_i \, \hat{a}_\theta$. If r_j is the radius of the energy harvesting coil with N_2 number of turns,

$$\psi = \int_{j=R_1}^{R_{N2}} \int_0^{2\pi} (B_r \cos \theta_i - B_\theta \sin \theta_i) \cdot r_j dr_j d\varphi. \tag{13}$$
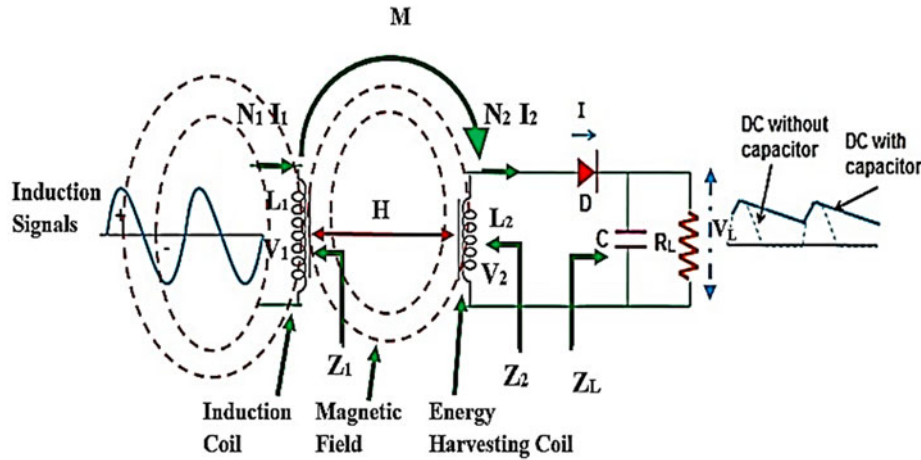
Figure 3. Equivalent circuit of the proposed MFEH system.

After putting the values of B_r and B_θ from Eqs. (10) and (11) into Eq. (12), the total flux is given as

$$\psi = \int_{j=R1}^{R_{N2}} \int_0^{2\pi} \left(\sum_{i=1}^{N_1} \frac{\mu_0 I R_i^2 2\cos\theta_i}{4\left|r_{p_i}\right|^3} \cos\theta_i \right. $$
$$\left. - \sum_{i=1}^{N_1} \frac{\mu_0 I R_i^2 \sin\theta_i}{4\left|r_{p_i}\right|^3} \sin\theta_i \right) . \, r_j dr_j d\varphi \qquad (14)$$

where current flow in induction coils is "I" and "ψ" is magnetic flux density generated over a small cross-section area (ds) from the center of the energy harvesting coil

$$\psi_r = \int_{j=R1}^{R_{N2}} \int_0^{2\pi} \left(\sum_{i=1}^{N_1} \frac{\mu_0 I R_i^2 2\cos\theta_i}{4\left|r_{p_i}\right|^3} \cos\theta_i \right) . \, r_j dr_j d\varphi \quad (15)$$

If the energy harvesting coil is placed above or below the induction coil at height (H_i), the angle θ_i is much smaller; therefore, the first term of Eq. (14) dominates, and the second term can be ignored. After the simplification, the modified equation is written as

$$\psi_\theta = - \int_{j=R1}^{R_{N2}} \int_0^{2\pi} \left(\sum_{i=1}^{N_1} \frac{\mu_0 I R_i^2 \sin\theta_i}{4\left|r_{p_i}\right|^3} \sin\theta_i \right) . \, r_j dr_j d\varphi \qquad (16)$$

When the energy harvesting coil is positioned as indicated in Fig. 4(a, b, d), the generated flux in the coil follows Eq. (15). The induced flux follows Eq. (16) if the energy collecting coil is positioned at the location shown in Fig. 4(c) since θ_i is substantially closer to 90°.

Experimental measurement

The prototype of the proposed low-cost MFEH system is shown in Fig. 2(a). There are 28 variable spiral coils in the circuit; each has 15 turns and measures 15.6 cm in diameter on the outside and 4.4 cm on the inside. These coils, which have a resistance of 0.2 Ω and an inductance of 100.68 μH, are used to absorb microwave emissions from the cooktop's main coil. The LCR meter is used for the measurement of coil resistance and inductance. A simple half-wave rectifier with a capacitor filter converts received RF energy of frequency 26 kHz to DC electrical voltage. In order to perform the experiment, an induction cooktop from Havells company with

Model no. INSTA COOK PT (230 V, 50 Hz, 120–1600 W) has been used. If we use different power levels on the induction cooktop, there is a small difference in the operation frequency. Through experimentation, it was found that when a utensil with a diameter of 14.5 cm and a height of 7.5 cm is used with a filled water level of 5.5 cm, the induction cooktop produces signals at a frequency of 24–32 kHz while cooking. The chosen induction functions in a variety of switching modes. Its operating frequency can switch between 0.5 kHz, 5 kHz, 25 kHz, and 30 kHz when the power level is less than 700 W, however, it often runs close to the 26 kHz frequency. Assume that the power level is 700 W or greater. Then, depending on the size of the utensil, the induction operates at a steady frequency of 26 kHz with a small fluctuation within the 24–32 kHz range.

The induced voltage generated by magnetic flux is influenced by the distance between the coils, turns in the coil, and location of the coil. As the distance between the induction and harvesting coils increases, mutual coupling decreases, reducing the induced voltage. A half-wave rectifier with a silicon 1N4007S diode, a 300 Ω load, and a 1 mF capacitor filter converts the induced voltage to a DC signal.

The entire circuit diagram for the suggested energy harvesting circuit is depicted in Fig. 3, where N_1 and N_2 represent the turns in the energy harvesting and induction coils, respectively. The coil's input impedance is Z_2, while the induction coil's input impedance is Z_1. Energy harvesting coils and induction coil impedance are connected as

$$Z_2 = \left\{ \frac{N_2}{N_1} \right\}^2 Z_1. \qquad (17)$$

The voltage V_1 (at induction coil) and V_2 (at harvesting coil) are

$$V_2 = L_2 \frac{dI_2}{dt} + M \frac{dI_1}{dt} \qquad (18)$$

$$V_1 = L_1 \frac{dI_1}{dt} + M \frac{dI_2}{dt} \qquad (19)$$

In this case, M is the mutual inductance between the coils, L_1 and L_2 are the inductance, and I_1 and I_2 are the currents in the coils.

If r_d is the forward bias diode resistance, then for maximum power transfer from source to load resistance (R_L), the impedance
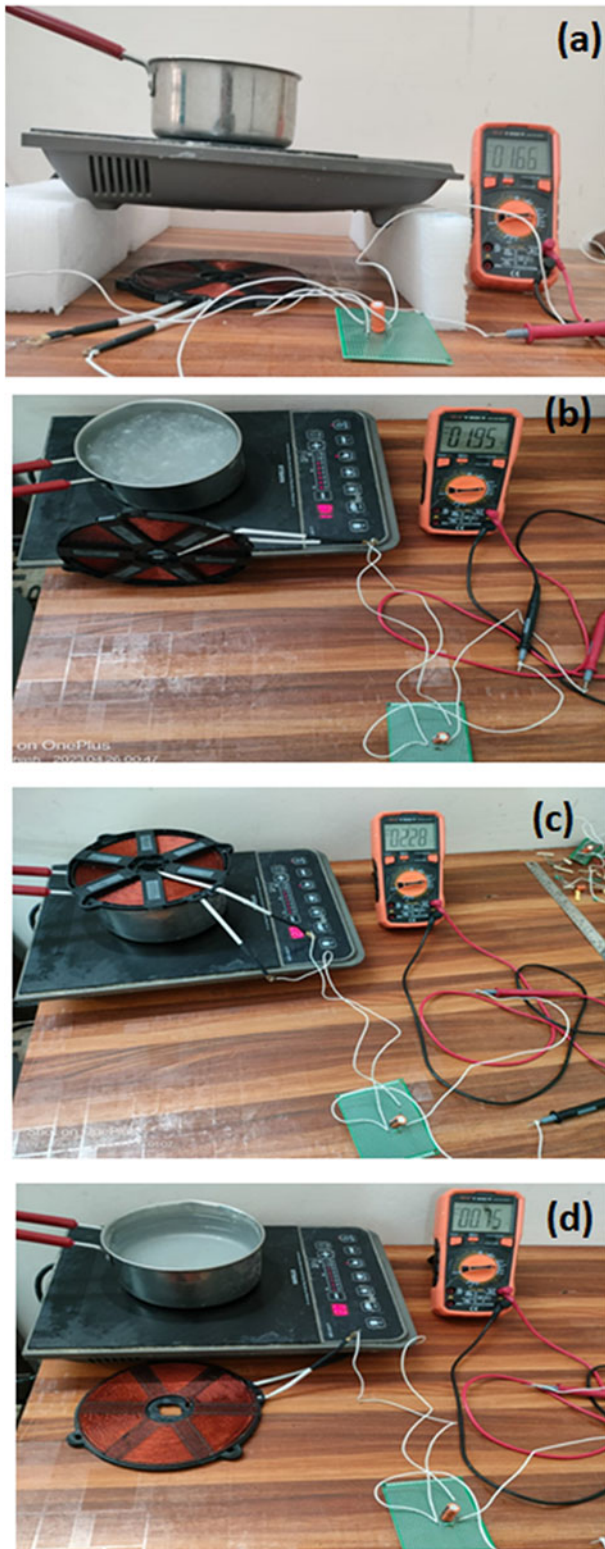
Figure 4. Measurement of DC voltage across the load resistance for various positions of the proposed circuit as shown in 4(a-d).

of the energy harvesting coil (Z_2) and diode forward bias resistance (r_d) are complex conjugates with load impedance (Z_L) and given as

$$Z_L^* = Z_2 + r_d. \tag{20}$$

The input impedance (Z_2) of the energy harvesting coil is equal to the induction coil impedance (Z_1) since the induction coil and energy harvesting coils are nearly equivalent ($L = 100\ \mu H$; $R = 0.2\ \Omega$) and the induction coil's number of turns (N_1) is roughly equal to that of the energy harvesting coil (N_2). In situations where the load impedance and the energy harvesting coil (Z_2) impedance are complicated and affect one another, the maximum power transfer from induction coils to load resistance (R_L) occurs. Another way to express Eq. (20) in terms of resistance and inductance is as follows:

$$R_{coil} + r_d + j\omega L_2 = \frac{R_L\,(1 + j\omega R_L C)}{1 + \omega^2 R_L^2 C^2}. \tag{21}$$

Now, comparing the real part on both sides, we get

$$R_{coil} + r_d = \frac{R_L}{1 + \omega^2 R_L^2 C^2}. \tag{22}$$

Since $\omega^2 R_L^2 C^2 \gg 1$, thus

$$R_{coil} + r_d = \frac{1}{\omega^2 R_L C^2} \tag{23}$$

As $R_{coil} \ll r_d$

$$r_d = \frac{1}{\omega^2 R_L C^2}. \tag{24}$$

Similarly, by comparing the imaginary part of Eq. (20), we get

$$L_2 = \frac{R_L^2 C}{1 + \omega^2 R_L^2 C^2}. \tag{25}$$

Since $\omega^2 R_L^2 C^2 \gg 1$, thus

$$L_2 = \frac{1}{\omega^2 C}. \tag{26}$$

Therefore, Eqs. (24) and (26) make it simple to forecast how load impedance (Z_L) will behave for maximum power transfer. The symbol for the maximum power transfer across the load is

$$P_L = \frac{V_2^2}{4 R_L}. \tag{27}$$

Ripple voltage across the load resistor is given by

$$V_r = \frac{V_L}{f R_L C}. \tag{28}$$

The mutual inductance between these two coils determines the maximum power transmission from induction coils to energy harvesting coils. The mutual inductance is greatest when the induction coils are close to one another, and it lowers when the coils move apart. Several frequency signals (24–32 kHz) are produced by the induction cooktop based on the size of the utensil, the applied power level, and the water level height. However, if induction is active above the 700 W power threshold, it typically functions at 26 kHz. We measured the DC load voltage in the experiments for various load resistors at different positions and other places where the induction cooktop's energy-collecting coils were located.

Results and discussions

Figure 4 shows voltage measurements across various load resistors (R_L) with different energy-collecting coil placements. In Fig. 4(a), the coil is positioned at a distance "H" beneath the induction cooktop, and power is measured at various distances. In Fig. 4(b), the coil is vertically atop the cooktop, and in Fig. 4(c), it is above a

Table 1. Measured voltage across different load resistance R_L with constant value of $C = 1\ mF$ at various positions of the coil

Utensil position	Harvesting coil position	Measured DC voltage (V_L) across load resistor (R_L) in V							
		$R_L = 11.8\ \Omega$	$R_L = 33\ \Omega$	$R_L = 46.6\ \Omega$	$R_L = 55.6\ \Omega$	$R_L = 68\ \Omega$	$R_L = 99\ \Omega$	$R_L = 178\ \Omega$	$R_L = 300\ \Omega$
Fig. 4(a)	$H = 7.0$ cm below	1.26–1.28	1.886–1.89	2.56–2.58	2.80–2.84	2.28–2.32	3.45–3.5	4.10–4.20	4.50–4.60
Fig. 4(a)	$H = 4.5$ cm below	2.45–2.47	3.92–3.96	4.56–4.62	5.35–5.40	5.60–5.70	6.70–6.80	8.10–8.20	8.20–8.25
Fig. 4(a)	$H = 2.0$ cm below	4.85–4.90	7.31–7.41	9.40–9.60	10.30–10.40	10.70–10.90	12.75–12.85	15.10–15.50	15.10–15.30
Fig. 4(a)	$H = 0$	–	–	–	–	13.0–13.5	14.5–15.5	18.2–18.6	22.2–22.4
Fig. 4(b)	Horizontally on table	0.180–0.182	0.40–0.41	0.40–0.41	0.428–0.430	0.40–0.42	0.63–0.64	0.73–0.74	0.75–0.76
Fig. 4(c)	Vertically on table	0.705–0.715	1.30–1.34	1.40–1.42	1.52–1.55	1.52–1.55	1.94–1.95	2.08–2.10	2.08–2.10
Fig. 4(d)	$H = 7.5$ cm Top on utensil	0.573–0.576	1.04–1.07	1.40–1.42	1.40–1.42	1.65–1.70	1.65–1.70	1.90–1.95	2.16–2.20

Table 2. Measured average DC power across the different load resistance R_L with constant value of $C = 1\ mF$ at various positions of the coils

Utensil position	Position of harvesting coil	DC power (P_L) in mW							
		$R_L = 11.8\ \Omega$	$R_L = 33\ \Omega$	$R_L = 46.6\ \Omega$	$R_L = 55.6\ \Omega$	$R_L = 68\ \Omega$	$R_L = 99\ \Omega$	$R_L = 178\ \Omega$	$R_L = 300\ \Omega$
Fig. 4(a)	$H = 7.0$ cm	136	108	141.7	143	77.7	121	96.7	69
Fig. 4(a)	$H = 4.5$ cm	512	470	454	520	469	460	373	224
Fig. 4(a)	$H = 2.0$ cm	2000	1637	1936	1926	1715	1654	1315	1100
Fig. 4(a)	$H = $ Nil	–	–	–	–	2580	2270	1902	1657
Fig. 4(b)	Horizontal on table	2.77	4.8	3.6	3.3	2.47	4.0	3	1.9
Fig. 4(c)	Vertical on table	42.7	52.8	42.6	42.1	42.1	38.4	24.54	15.8
Fig. 4(d)	$H = 7.5$ cm over top of utensil	28	33	42.6	42.6	41.0	34.1	21	17.6

water-filled utensil. In Fig. 4(d), the coil is on the table horizontally. The magnetic field from the induction coils heats the steel utensil and water (24–32 kHz). The energy-harvesting circuit captures magnetic energy leakage under the cooktop, converting it to DC for storage in a battery, which can power devices like smartphones, LED lights, and IoT devices. For the various locations of the coils as indicated in Fig. 4, the voltage measured at the various load resistors (R_L) with $C = 1$ mF is tabulated in Table 1. An average voltage of 4.85–4.9 V is created across an 11.8 Ω load resistor at a height of 2 cm below the induction cooktop, as indicated in Fig. 4(a). According to Table 1, when the vertical distance increases, the developed voltage decreases. The voltage drops to 1.26–1.28 V at a height of 7 cm. Figure 4(b) shows the location of the harvesting coil, where a minimum voltage of 0.18 V is detected because of less magnetic field coupling in the harvesting coil. Furthermore, as Table 1, illustrates, an increase in voltage is seen if the energy harvesting coil is positioned at the location shown in Fig. 4(c). For every position shown in Fig. 4, the voltage across the load rises as the load resistance rises. It was noted that at values of $R_L < 68$ Ω,

the load resistance was harmed at $H = 0$ mm. Consequently, when $H = 0$ mm and $R_L \geq 68$ Ω, the maximum voltage across the load is observed.

Table 2 shows the average DC power measured across various load resistances with $C = 1$ mF for different harvesting coil placements in Fig. 4. For $R_L = 11.8$ Ω, an average DC power of 2000 mW is noted at $H = 2$ cm (Fig. 4(a)). As the distance increases, load power decreases, reaching a minimum of 2.77 mW at the position in Fig. 4(b). Power levels of 42.7 mW and 28 mW are observed for Fig. 4(c) and 4(d), respectively. When the coil is positioned in Fig. 4(a) at $H = 0$ mm, $R_L \geq 68$ Ω shows a high average DC load power of 2580 mW. Figure 5(a) displays the average DC power across different load resistances for $C = 1$ mF with coils positioned at various heights below the cooktop, as shown in Fig. 4(a). Figure 5(a) shows that the power level across the load resistor drops as the load resistor R_L value rises. The load resister $R_L = 68$ Ω displays an average DC load power of 2586 mW for $H = 0$ mm, while the load resister $R_L = 300$ Ω displays a load power measurement of 1657 mW. Since high power across the load burns
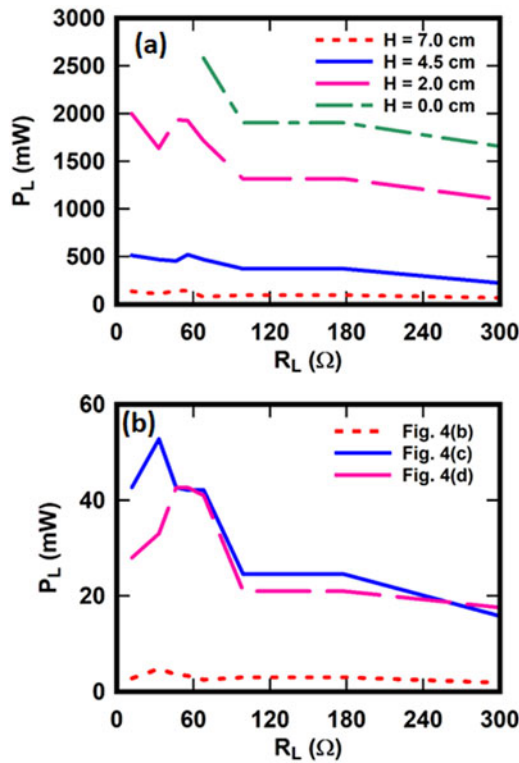
Figure 5. DC power measurement across various load resistance (a) for various heights (*H*) when the coil is located as shown in Figure 4(a); (b) for various positions of the coil shown in Figure 4(b, c, d).
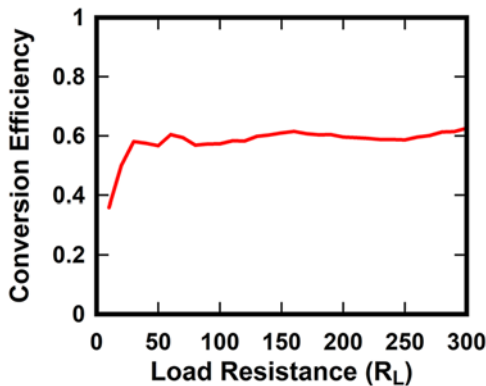

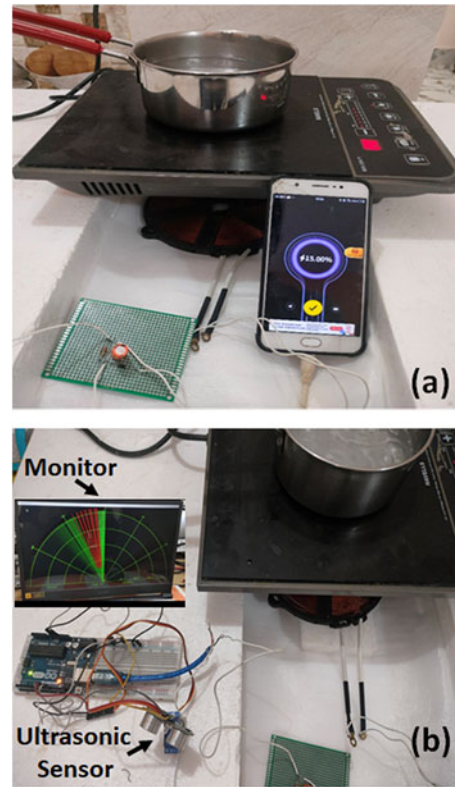**Figure 6.** Effect of load resistance on the conversion efficiency of the proposed MFEH circuit.

Figure 7. Demonstration of wireless powering when the harvesting coil is placed at a position shown in Figure 4(a): (a) mobile phone (VIVO Y69) charging when $H = 7$ cm, (b) powering low power IoT-based sensor.

For $H = 4.5$ cm, the power level across the load $R_L = 11.8$ Ω is 512 mW. The power decreases to 454 mW at $R_L = 46.6$ Ω, then increases to 520 mW at $R_L = 55.6$ Ω due to improved impedance matching. Figure 5(b) shows the average power for different coil placements. At $R_L = 11.8$ Ω, the arrangement in Fig. 4(b) yields 2.77 mW, rising to 4.8 mW at $R_L = 33$ Ω. Power variance is due to impedance matching. In Fig. 4(c, d), power initially rises and then falls as load resistance increases. The conversion efficiency of the proposed circuit with different load resistance is calculated and plotted as shown in Fig. 6. It has been observed that for lower load resistance of 15 Ω, the conversion efficiency is near 40%. However, it varies from 55 to 65% for the load resistance of 30–300 Ω.

Practical demonstration

Figure 7 illustrates how the intended harvesting circuit powers the IoT-based sensor and charges the mobile device. The capacitance $C = 1$ mF and load resistance $R_L = 2.2$ MΩ are connected across the device in all practical examples. As seen in Fig. 4(a), we placed energy-collecting coils for mobile charging applications at a height of $H = 7$ cm below the induction cooktop. Because the mobile phone model VIVO-Y69 has a high impedance of 16.7 kΩ, we have utilized high load resistance $R_L = 2.2$ MΩ in this case. As a result, when the phone and load resistance are linked in parallel, the phone experiences maximum current flow, which initiates the charging process. Because of the high load resistance, a steady DC voltage of 10.93 V with very little ripple voltage is seen across the load. As illustrated in Fig. 7(b), we also provide our harvesting circuit for supplying power to the low-power IoT sensor. Here, we powered from the suggested circuit to an IoT-based project

the load resister for $H = 0$ mm, we did not measure power for $R_L < 68$ Ω. Similarly, the load power level for $H \in [2, 4.5, 7]$cm when $R_L \in [11.8, 33, 46.6, 55.6, 68, 99, 178, 300]$ Ω is plotted in Fig. 5(a). The measured dc power for $R_L = 11.8$ Ω at $H = 2.0$ cm is roughly 2000 mW. In contrast, a dc power of 1650 mW is seen at 33 Ω, and when the load resister is increased from 46.6 Ω to 55.6 Ω, this power level rises once again to 1900 mW. Impedance matching has improved, which is the cause of the rise in load power. The average dc load power across the load resister $R_L = 55.6$ Ω for $H = 7$ cm is roughly 143 mW; however, the power level drops as the load resister R_L is increased or decreased because of the impedance mismatch between the load and the energy harvesting coil's output.

Table 3. Comparison of proposed work with similar other works

Ref. No.	Magnetic energy source	Operating frequency	AC to DC circuit	Load power
[20]	Railway track	50 Hz	NA	40.6 mW, AC
[21]	Railway track	50 Hz	NA	3.8 mW, AC
[22]	AC power line	50 Hz	Silicon diode (FWR)	0.18 mW, DC
This work	Induction cooktop	26 kHz	Silicon diode (HWR)	2580 mW, DC

comprising Arduino Una, a servomotor, and an ultrasonic sensor. This system uses an ultrasonic sensor and servo motor to detect the movement of any object in its path. It then displays the detected object's location in red on the computer monitor.

The energy harvesting coil is positioned for demonstration at a height $H = 4$ cm beneath the induction cooktop (refer to Fig. 7(b)). The load resister, $R_L = 2.2$MΩ, is now connected in parallel to the IoT device, which has an input impedance of 2.4 MΩ. As seen in the inset of Fig. 7(b), this supplies power to the sensor, which rotates with the aid of a servo motor and transmits the signal to the computer monitor. In this instance, a DC value of 20.2 V is noted across the $R_L = 2.2$ MΩ load resistor. As a result, our suggested device can supply future smart houses with low-power IoT devices. For experimental demonstration, the proposed circuit is made on a PCB prototype board which makes the system relatively large. However, the circuit can be easily scaled to a small size by designing the rectifier circuit on PCB and using the dry etching technique.

The comparison of the proposed work with the similar work is illustrated in Table 3. It has been cleared from Table 3 that the railway track line and AC power lines were used in the past to harvest the magnetic energy. Furthermore, with our proposed circuit, a maximum power of 2580 mW, DC can be obtained by placing the coil near the induction cooktops with a load resistance of 68 Ω. This much power was not harvested in the previous works. Therefore, our proposed circuit and methods are novel and have many advantages in comparison to previously reported work.

Conclusions

A simple MFE harvester circuit for powering low-power IoT based devices and mobile charging has been presented in this paper. The proposed device harnesses leaked MFE from induction cooktops used in daily kitchen activities. Through extensive experimentation across various positions, significant results have been achieved: at close proximity (within 2 cm), power output peaked at 1936 mW with voltage ranging from 9.4 V to 9.6 V using $C = 1$ mF and $R = 46.6$ Ω. Furthermore, it has been observed that load power decreases as load resistance increases, though optimal matching between the load and source can enhance power output at lower resistances. Positioning of the harvesting coil also affects power capture; placing it at certain heights yielded higher efficiencies compared to orthogonal placements. The proposed circuit has been demonstrated to charge mobile devices and powers the low-power IoT device, making it ideal for smart home applications. This unique capability to harvest MFE from induction cooktops distinguishes our device from previous magnetic harvesting circuits.

1. Dr Subash Chandra Yadav
2. Dr Rajan Agrahari.

References

1. **Chu S and Majumdar A** (2012) Opportunities and challenges for a sustainable energy future. *Nature* **488**(7411), 294–303. doi: 10.1038/nature11475

2. "Building a sustainable energy future," National Science Foundation, Arlington County, VA, USA, Tech. Rep. NSB-09-35, 2009.

3. **Sisinni E, Saifullah A, Han S, Jennehag U and Gidlund M** (2018) Industrial internet of things: Challenges, opportunities, and directions. *IEEE Transactions on Industrial Informatics* **14**(11), 4724–4734. doi: 10.1109/TII.2018.2852491

4. **Makhdoom I, Abolhasan M, Lipman J, Liu RP and Ni W** (2019) Anatomy of threats to the Internet of things. *IEEE Communications Surveys and Tutorials* **21**(2), 1636–1675. doi: 10.1109/COMST.2018.2874978

5. **Amiri M, Tofigh F, Shariati N, Lipman J and Abolhasan M** (2021) Review on metamaterial perfect absorbers and their applications to IoT. *IEEE Internet of Things Journal* **8**(6), 4105–4131. doi: 10.1109/JIOT.2020.3025585

6. **Agrahari R, Singh S, Samantaray D, Kumar B, Bhattacharyya S, Mahto M and Jain PK** (2023) Triple-band metasurface absorber for RF energy harvesting applications. *Microwave and Optical Technology Letters* **65**(8), 2252–2261. doi: 10.1002/mop.33728

7. **Lozinskii MG** (1969) *Industrial Applications of Induction Heating*, 1st English Edn. New York, NY, USA: Pergamon.

8. **Moreland WC** (1973) The induction range: Its performance and its development problems. *IEEE Transactions on Industry Applications* **9**(1), 81–85. doi: 10.1109/TIA.1973.349892

9. **Stauffer PR, Cetas TC and Jones RC** (1984) Magnetic induction heating of ferromagnetic implants for inducing localized hyperthermia in deep-seated tumors. *IEEE Transactions on Biomedical Engineering* **BME-31**(2), 235–251. doi: 10.1109/TBME.1984.325334

10. **Wang ZL** (2013) Nanogenerators as new energy technology for self-powered systems and as active mechanical and chemical sensors. *ACS Nano* **7**(11), 9533–9557. doi: 10.1021/nn404614z

11. **Jeong CK, Lee J, Han S, Ryu J, Hwang GT, Park DY, Park JH, Lee SS, Byun M, Ko SH and Lee KJ** (2015) A hyper-stretchable elastic-composite energy harvester. *Advanced Materials* **27**(18), 2866–2875. doi: 10.1002/adma.201500367

12. **Hwang GT, Annapureddy V, Han JH, Joe DJ, Baek C, Park DY, Kim DH, Park JH, Jeong CK, Park KI and Choi JJ** (2016) Self-powered wireless sensor node enabled by an aerosol-deposited PZT flexible energy harvester. *Advanced Energy Materials* **6**(13), 1600237. doi: 10.1002/aenm.201600237

13. **Xu B, Chakraborty H, Remsing RC, Klein ML and Ren S** (2017) A free-standing molecular spin–charge converter for ubiquitous magnetic-energy harvesting and sensing. *Advanced Materials* **29**(8), 1605150. doi: 10.1002/adma.201605150

14. **Yang F, Du L, Yu H and Huang P** (2020) Magnetic and electric energy harvesting technologies in power grids: A review. *Sensors* **20**(5), 1496. doi: 10.3390/s20051496

15. **Yuan S, Huang Y, Zhou J, Xu Q, Song C and Yuan G** (2017) A high-efficiency helical core for magnetic field energy harvesting. *IEEE Transactions on Power Electronics* **32**(7), 5365–5376. doi: 10.1109/TPEL.2016.2610323

16. **Jiang W, Lu J, Hashimoto S and Lin Z**, A non-intrusive magnetic energy scavenger for renewable power generation state monitoring, in *Proc. IEEE Int. Conf. Renewable Energy Res. Appl.*, Birmingham, U.K., 2016, 562–566.

17. **Wu Z, Nguyen DS, White RM, Wright PK, O'Toole G and Stetter JR** (2018) Electromagnetic energy harvester for atmospheric sensors on overhead power distribution lines. *Journal of Physics: Conference Series* **1052**(1), 1–4.

18. **Yuan S, Huang Y, Zhou J, Xu Q, Song C and Thompson P** (2015) Magnetic field energy harvesting under overhead power lines. *IEEE Transactions on Power Electronics* **30**(11), 6191–6202. doi: 10.1109/TPEL.2015.2436702

19. **Kuang Y, Chew ZJ, Ruan T, Lane T, Allen B, Nayar B and Zhu M** (2021) Magnetic field energy harvesting from the traction return current in rail tracks. *Applied Energy* **292**, 1–14. doi: 10.1016/j.apenergy.2021.116911

20. **Espe AE, Haugan TS and Mathisen G** (2022) Magnetic field energy harvesting in railway. *IEEE Transactions on Power Electronics* **37**(7), 8659–8668. doi: 10.1109/TPEL.2022.3141437

21. **Kuang Y, Chew ZJ, Ruan T and Zhu M** (2021) Magnetic field energy harvesting from current-carrying structures: Electromagnetic-circuit coupled model, validation and application. *IEEE Access* **9**, 46280–46291. doi: 10.1109/ACCESS.2021.3068472

22. **Hosseinimehr T and Tabesh A** (2016) Magnetic field energy harvesting from AC lines for powering wireless sensor nodes in smart grids. *IEEE Transactions on Industrial Electronics* **63**(8), 4947–4954.

Dr Subash Chandra Yadav is currently working as an assistant professor in the department of Electronics and Communication Engineering NIT Patna Bihar India. He has completed M.Tech degree in RF and Microwave Engineering from IIT Kharagpur in 2013 and PhD degree in RF and Microwave Engineering from IIT Bombay in 2021. He worked on broadband microstrip antenna during his PhD work and he has published more than 11 SCI Index Journals Papers. Currently he is working as high gain substrate integrated antennas integrated with planner dielectric lens.

Dr Rajan Agrahari is currently working as an assistant professor in the department of Electronics and Communication Engineering NIT Patna Bihar India. He has completed PhD degree in RF and Microwave Engineering from IIT BHU in 2019. He worked on metamaterial and metasurfaces during his phd thesis. He has published more than 15 SCI index Journal snd 5 indian patents.